Triggering and probing electromagnetic stochasticity in a low-density magnetized plasma irradiated by a multi-speckled laser beam

Contact: julien.fuchs@polytechnique.edu

W. Yao
LULI - CNRS; École Polytechnique, CEA; Université Paris-Saclay; UPMC Université Paris 06; Sorbonne Université, F-91128, Palaiseau Cedex, France

P. Antici
INRS-EMT, 1650 boul, Lionel-Boulet, Varennes, QC, J3X 1S2, Canada

J. Béard
LNCMI-T, CNRS, Toulouse, France

M. Borghesi
Center for Plasma Physics, School of Mathematics and Physics, Queen's University Belfast, Belfast BT7 1NN, United Kingdom

A. F. A. Bott
Department of Physics, University of Oxford, Parks Road, Oxford OX1 3PU, UK.

D. C. Carroll
Central Laser Facility, STFC Rutherford Appleton Laboratory, Didcot, UK

S. N. Chen
"Horia Hulubei" National Institute for Physics and Nuclear Engineering, 30 Reactorului Street, RO-077125, Bucharest-Magurele, Romania

A. Ciardi
Sorbonne Université, Observatoire de Paris, Université PSL, CNRS, LERMA, F-75005, Paris, France

C. Fegan
Center for Plasma Physics, School of Mathematics and Physics, Queen's University Belfast, Belfast BT7 1NN, United Kingdom

L. Gremillet
CEA, DAM, DIF, F-91297 Arpajon, France

E. d'Humières
University of Bordeaux, Centre Lasers Intenses et Applications, CNRS, CEA, UMR 5107, F-33405 Talence, France

B. Khiar
Office National d'Etudes et de Recherches Aérospatiales (ONERA), Palaiseau 91123, France

R. Lelièvre
LULI - CNRS; École Polytechnique, CEA; Université Paris-Saclay; UPMC Université Paris 06; Sorbonne Université, F-91128, Palaiseau Cedex, France

P. Martin
Center for Plasma Physics, School of Mathematics and Physics, Queen's University Belfast, Belfast BT7 1NN, United Kingdom

A. McIlvenny
Center for Plasma Physics, School of Mathematics and Physics, Queen's University Belfast, Belfast BT7 1NN, United Kingdom

R. Smets
Laboratoire de Physique des Plasmas (LPP), CNRS, Observatoire de Paris, Sorbonne Université, Université Paris-Saclay, École Polytechnique, Institut Polytechnique de Paris, 91120 Palaiseau, France

J. Fuchs
LULI - CNRS; École Polytechnique, CEA; Université Paris-Saclay; UPMC Université Paris 06; Sorbonne Université, F-91128, Palaiseau Cedex, France

Abstract

The triggering of electromagnetic stochasticity in magnetized plasmas via high-power lasers is investigated by sending a nanosecond-duration, multi-speckled laser pulse into a low-density gas, coupled with a strong, initially homogeneous, external magnetic field perpendicular to the laser pulse. Detailed characterization of the induced electromagnetic structures is realized through proton radiography, in addition to Thomson scattering measurements for the background plasma heating. The experiment is performed using an intense short-pulse laser and several long-pulse lasers, at the Vulcan Target Area West laser facility at the Rutherford Appleton Laboratory. Additionally, the energy spectrum of MeV protons propagated through the plasma is registered with a Thomson parabola. This allows us to assess the impact of the stochastic EM structures in the plasma on the transport of the collisionless proton beam.

1 Introduction

Turbulence is the natural state of many space and astrophysical systems [1], such as the solar wind [2], interstellar medium [3], [4], and galaxy clusters [5]. With its ubiquitous prevalence, plasma turbulence is believed to play an important role in the amplification of magnetic fields [6] and in the acceleration and transport of

energetic particles [7].

Investigating plasma turbulence with high-power lasers has become a hot topic recently, e.g., in the collective interaction between intense proton beams and unmagnetized plasma [8], the propagation of energetic charged particles through laser-produced magnetized plasmas [9], and the collision of laser-produced plasma flows, without [10], or with [11] externally applied magnetic fields. Here we report on an experiment whereby stochastic electromagnetic (EM) structures were generated in a plasma in a different manner than in previous works. Indeed, the efforts discussed above investigated how to seed and amplify turbulence in plasmas. Here, we start from imposing a strong, homogeneous magnetization onto the plasma, and examine how to break it down to a stochastic structure, while keeping local strong fields. Stochastisation is here seeded by propagating a multi-speckled laser (in contrast to a "single"-speckled Gaussian one [12]) in the magnetized plasma.

2 Experiments

2.1 Setup

This experiment was carried out at the Vulcan Target Area West (TAW) laser facility at the Rutherford Appleton Laboratory (RAL), where we exploit its multi-beam capability. As sketched in Fig. 1 (a), a long pulse multi-speckled beam (propagating along the x-axis) was used to ionize and heat a low-density gas (Neon), which was injected from the gas nozzle located at the target chamber center (TCC). The gas flow is along the z-axis. Additionally, a frequency-converted long-pulse laser (following the same path as the main ionizing long-pulse laser), was used to perform Thomson scattering (TS) measurements. Fig. 1 (b) shows the experimental arrangement near TCC. A short-pulse laser beam (red, along the y-axis) was used to generate the energetic proton beams for proton radiography via target normal sheath acceleration (TNSA) [13], [14]. The broadband proton beam was generated by a foil target placed at a distance of $d = 2.4$ or 17.4 mm from the peak of the pre-ionized gas jet. Details of the foil are shown in the dashed circle below. Two diagnostics were deployed at the end of the y-axis, i.e., a Thomson parabola (TP) and radiochromic films (RCF), to diagnose the TNSA-produced proton beam. The latter was located at a distance around 6.4 cm from TCC. The whole setup was embedded in an external magnetic field (yellow arrow), generated from the Helmholtz coil system [15], [16], shown in Fig. 1 (a). This field was along the y-axis, the same as the short pulse laser.

The ns laser was positioned at a height of $h = 2$ mm above the gas nozzle. At this height, the gas jet had a Gaussian density profile, characterized by a 2 mm full-width-at-half-maximum (FWHM) and a peak density of 10^{18} cm^{-3}/bar (for the neutral gas). Since the magnetic field extends homogeneously over $\sim$5 cm longitudinally [15], it can be considered uniform at the scale of the gas jet. A magnetic as strong as 30 T can be applied to the setup. We verified that, as expected, since the magnetic field is aligned with the TNSA proton beam main axis, the proton beam is not affected by the magnetization (which starts a few μs before the short-pulse irradiates the target). Note that, as shown in Fig. 1 (c), the multi-speckled ns-laser has an elliptical focal spot 2 mm (along y) $\times$ 200 μm (along z, these values are given foot-to-foot), while each speckle is measured to be around 30 μm.

2.2 Proton radiography results

An example of raw data of proton radiography is shown in Fig. 2. Without the external magnetic field, the RCF shows a very clean proton source, on top of which we can also clearly recognize the long pulse laser path, as can be seen in panel (a). Note that the blue arrow on the right shows the ionizing laser direction. The pattern observed on the RCF is caused by the ponderomotive electric field of the laser envelope [17]. Furthermore, the pattern also indicates self-focusing and filamentation of the laser pulse, as expected in such conditions [18].

When applying a magnetic field of 30 T, it is clear that the simple pattern becomes complex, with a large dark pattern in the middle, surrounded by several "net"-shaped structures, as shown in panel (b). We have scanned the magnetic field strength from 5 T up to 30 T, and found that with the increase of the magnetic field strength, the "net"-shaped structure becomes more visible and chaotic. Such "net"-shaped structure likely results from a distributed EM structure within the plasma.

We will further analyse the proton radiography results with the code PROBLEM [19], in order to better characterize the magnetized plasma quantitatively, i.e., to find the values of the following important parameters and understand the regime the plasma is in:

1. the turbulent Mach number $Ma_{turb} \equiv u_{rms}/c_s$, where c_s is the sound velocity of the plasma, and u_{rms} is the velocity of the bulk motion of the magnetized plasma;

2. the magnetic Reynolds number $R_m \equiv u_{rms}L/\eta$, where L is the characteristic length scale of the magnetized plasma and η is the plasma resistivity;

3. the magnetic Prandtl number $Pm \equiv Rm/Re$, where $Re \equiv u_{rms}L/\nu$ is the fluid Reynolds number and ν is the kinematic viscosity of the fluid.

The velocity u_{rms} could be extracted from the RCF results [20], while the plasma's viscosity and resistivity will be estimated following a similar procedure detailed in the supplementary material of [20]. The temperature and density are extracted from the TS diagnostics detailed below.

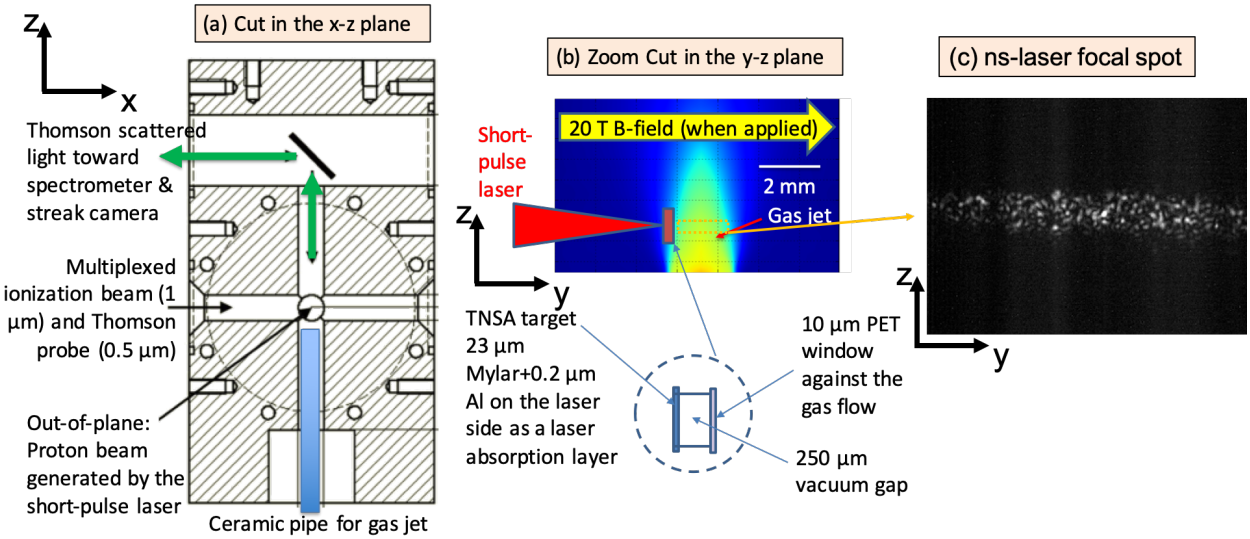

Figure 1: **Experimental setup.** (a) Side view of the overall experimental arrangement inside the assembly of the coil generating the pulsed magnetic field (the $x-z$ plane). A long-pulse, multi-speckled beam (70 J, 1 ns square shape, 1 μm wavelength, with an elliptical focal spot of 2 mm $\times$ 200 μm, at an intensity of around 1.1×10^{13} W/cm^2) is sent, along the x-axis to ionize and heat the gas jet. A 0.5 μm wavelength TS probe beam, co-propagating with the ns-ionizing laser, is used to characterize the density and temperature of the heated gas, and the Thomson scattered light is collected at 90° by a set of spectrometers and streak cameras. (b) The detailed experimental arrangement around the TCC in the $y-z$ plane. A low-density gas jet is injected around the TCC along the z-axis. Neon is used for the gas, under various pressures (2/5/10/25 bars). The colormap (from blue to red) represents the gas density profile (from low to high). A strong magnetic field (5/10/20/30 T) is applied along the y-axis. A short pulse beam (150 J, 1 ps Gaussian duration FWHM, with a focal spot diameter of 40 μm, at an intensity of around 1.2×10^{19} W/cm^2) irradiates a foil target, along the y-axis, to generate energetic protons. Details about the foil are shown in the dashed circle below. (c) An example of the gas-ionising, multi-speckled laser focal spot.

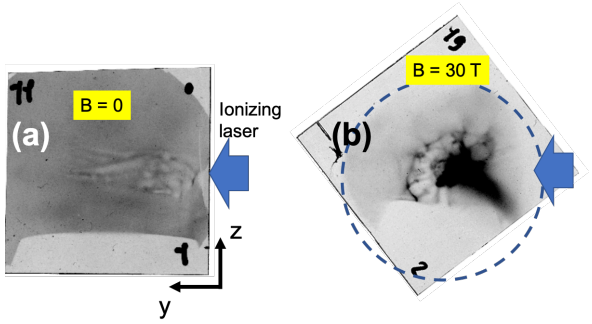

Figure 2: **Proton radiography results** (a) without and (b) with external applied magnetic field. In both cases the gas pressure is 25 bars, and the time delay (between the long, ionizing beam and the short pulse beam that drives the probing protons) is 0.7 ns.

2.3 Thomson scattering results

TS measurements allow us to characterize the background plasma conditions. By fitting the TS raw data of Fig. 3, we can infer the electron plasma density $n_e = 4 \times 10^{18}$ cm^{-3}, the electron temperature $T_e = 200$ eV, the ion temperature $T_i = 140$ eV, and the ionization state $Z^\star \sim 8$ (consistent with the ionization state predicted by FLYCHK [21] for such temperatures). These measurements have been used as input to the numerical simulations presented below.

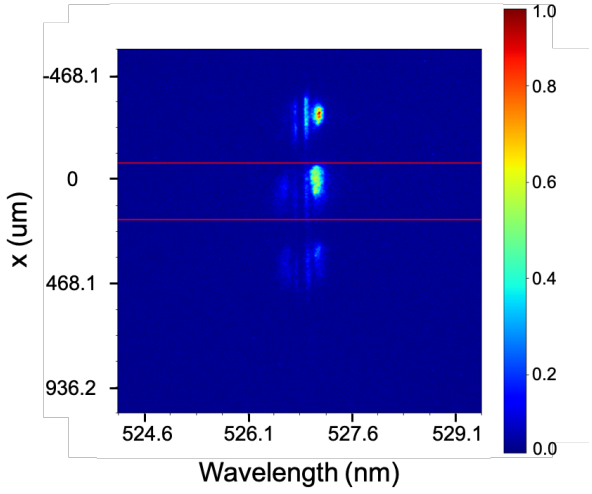

Figure 3: **Example raw data of the TS ion measurement.** The three spectra correspond to sampling those different locations along the x-axis. Preliminary fitting of the signal averaged along the x-axis between the two red horizontal lines gives an estimate of $T_e = 200$ eV, $T_i = 140$ eV, $n_e = 4 \times 10^{18}$ cm^{-3}, and $Z_i = 8$. The colormap represents the normalized signal intensity.

2.4 Proton Spectra

As detailed in Fig. 1 (b), the TNSA-produced proton beam, which serves to radiograph the EM fields in the plasma, could alternatively be sent to a TP in order to analyze finely its spectrum after propagation through the plasma.

Figure 4 shows two proton spectra recorded in the experiment. When the proton beam propagates through the unmagnetized plasma (created by the ns laser), we see a typical TNSA spectrum with a ~ 8 Me cutoff energy. This spectrum is similar to that recorded in the absence of the dilute plasma, as is expected given the negligible stopping power of the plasma. However, when applying a 20 T magnetic field, a clear "bunching" of the spectrum can be seen, i.e., the cutoff energy reduces to ~ 4 MeV and a peak appears at ~ 0.7 MeV.

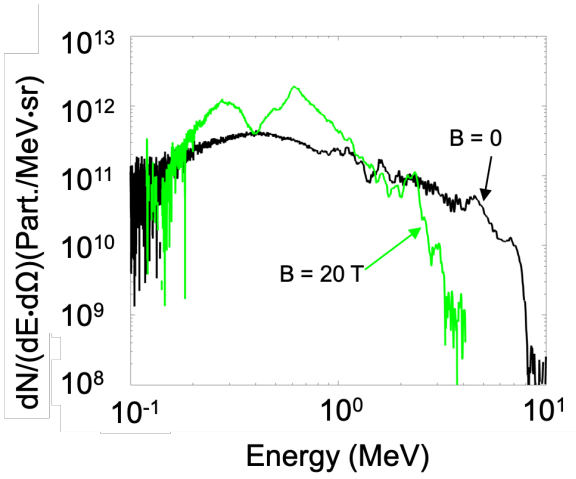

Figure 4: **Proton spectra** recorded with (green) or without (black) magnetic field.

Since we do not expect significant energy losses in the plasma, the reduced cutoff energy could be simply related to angular scattering. Since the highest energy part of the TNSA proton is associated with a narrow cone [22], the scattering could make them miss the entrance into the TP.

We will now turn to numerical simulations in order to interpret these results.

3 Simulations

To understand the prominent feature observed in the experiment (the presence of strong EM chaotic structures, inducing scattering of propagating protons), we will perform numerical investigations, using a set of complementary codes, e.g., magneto-hydrodynamic (MHD), hybrid, and kinetic, allowing us to investigate the underlying physics. Numerical results using the hybrid code HECKLE [23] (i.e. treating electrons as a fluid and ions

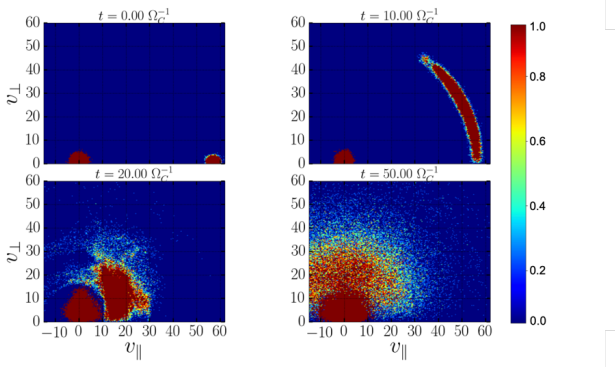

Figure 5: Simulation results, using the Heckle code, of the interaction of a streaming proton beam (having initial $v_\parallel = 55$, in unit of Alfvén speed, i.e. 300 keV) within a 20 T magnetized plasma (having initial $v_\parallel = 0$), as a function of time (in the unit of the inverse of the Lamor gyro-frequency Ω_C^{-1}). This shows the progressive isotropisation of the incoming proton beam. The colormap represents the normalized number of particles.

as particles), using conditions close to that of the experiment, are displayed in Fig. 5. This simulation indeed predicts a strong isotropisation of the initially directed proton beam, which translates into a reduced cutoff energy of the ion distribution collected by the the spectrometer. We will investigate this in more detail and compare it to the experimental results shown in Fig. 4.

In addition, to better understand the RCF results, we are in the process of performing MHD simulation with the code GORGON [24]. Taking advantage of a test-particle module, we can generate synthetic proton radiographs by sending an energetic proton source into the simulation box, whose trajectories will be deflected by the electromagnetic fields induced by the laser-gas interaction.

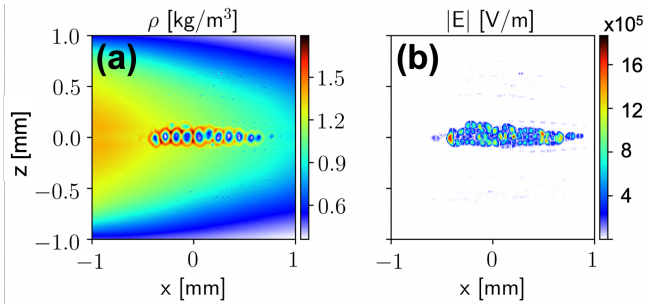

Figure 6: Simulation results of (a) mass density and (b) electric field strength, using the GORGON code with test particles, of the interaction of a multi-speckled ns-duration laser beam with the Neon gas (having the same laser parameters and gas profile) and in the presence of a 20 T magnetic field. The ionizing laser is directed out-of-plane along y.

To this goal, we need to calculate the electromagnetic field generated within the plasma during the multi-speckled laser-plasma interaction. Mimicking the multi-speckled laser used in the experiment, preliminary simulation results are shown in Fig. 6. We see that the multi-speckled laser creates density cavities inside the gas jet, which also results in hot spots with higher temperatures. More importantly, under a homogeneous magnetic field of 20 T, there are chaotic electric field structures associated with the density cavities (or the hot spots), which could form the seed for the "net"-shaped structure seen from the RCF.

Note that for now, the code only describes the induction electric field $\boldsymbol{E} = \boldsymbol{u} \times \boldsymbol{B}$. Once the Biermann battery term [25] is also treated, we will better model the field dynamics within the plasma. We will keep digging into this with better calibrated beam-plasma conditions from TS and also more advanced modelings [26].

4 Conclusion

To conclude, here we report the first attempt in triggering and probing EM stochasticity in a plasma, using a magnetized plasma irradiated by a multi-speckled laser. Various diagnostics are fielded in order to measure the plasma condition. RCF results exhibit strong chaotic structures but more analysis is needed to characterize the degree of EM stochasticity in the plasma. In addition, kinetic studies of the interaction between charged particles and the stochastic plasma are underway.

References

[1] S. Molokov, R. Moreau, K. Moffatt, A. A. Schekochihin, and S. C. Cowley, "Turbulence and magnetic fields in astrophysical plasmas," *Magnetohydrodynamics: Historical Evolution and Trends*, pp. 85–115, 2007.

[2] G. G. Howes, S. C. Cowley, W. Dorland, G. W. Hammett, E. Quataert, and A. A. Schekochihin, "A model of turbulence in magnetized plasmas: Implications for the dissipation range in the solar wind," *Journal of Geophysical Research: Space Physics*, vol. 113, no. A5, 2008.

[3] B. G. Elmegreen and J. Scalo, "Interstellar turbulence i: Observations and processes," *Annu. Rev. Astron. Astrophys.*, vol. 42, pp. 211–273, 2004.

[4] J. Scalo and B. G. Elmegreen, "Interstellar turbulence ii: Implications and effects," *Annu. Rev. Astron. Astrophys.*, vol. 42, pp. 275–316, 2004.

[5] F. Miniati, "The matryoshka run. ii. time-dependent turbulence statistics, stochastic particle acceleration, and microphysics impact in a massive galaxy cluster," *The Astrophysical Journal*, vol. 800, no. 1, p. 60, 2015.

[6] F. Rincon, F. Califano, A. A. Schekochihin, and F. Valentini, "Turbulent dynamo in a collisionless plasma," *Proceedings of the National Academy of Sciences*, vol. 113, no. 15, pp. 3950–3953, 2016.

[7] V. Zhdankin, G. R. Werner, D. A. Uzdensky, and M. C. Begelman, "Kinetic turbulence in relativistic plasma: From thermal bath to nonthermal continuum," *Physical Review Letters*, vol. 118, no. 5, p. 055 103, 2017.

[8] K. Mima, J. Fuchs, T. Taguchi, *et al.*, "Self-modulation and anomalous collective scattering of laser produced intense ion beam in plasmas," *Matter and Radiation at Extremes*, vol. 3, no. 3, pp. 127–134, 2018.

[9] L. Chen, A. Bott, P. Tzeferacos, *et al.*, "Stochastic transport of high-energy particles through a turbulent plasma," *The Astrophysical Journal*, 2020.

[10] P. Tzeferacos, A. Rigby, A. Bott, *et al.*, "Laboratory evidence of dynamo amplification of magnetic fields in a turbulent plasma," *Nature communications*, vol. 9, no. 1, p. 591, 2018.

[11] A. Bott, L. Chen, P. Tzeferacos, *et al.*, "Insensitivity of a turbulent laser-plasma dynamo to initial conditions," *Matter and Radiation at Extremes*, vol. 7, no. 4, p. 046 901, 2022.

[12] P. E. Masson-Laborde, S. Hüller, D. Pesme, *et al.*, "Stimulated brillouin scattering reduction induced by self-focusing for a single laser speckle interacting with an expanding plasma," *Physics of Plasmas*, vol. 21, no. 3, p. 032 703, Mar. 2014. DOI: 10.1063/1.4867659. [Online]. Available: https://doi.org/10.1063/1.4867659.

[13] S. Wilks, A. Langdon, T. Cowan, *et al.*, "Energetic proton generation in ultra-intense laser–solid interactions," *Physics of Plasmas*, vol. 8, no. 2, pp. 542–549, 2001.

[14] P. Mora, "Plasma expansion into a vacuum," *Physical Review Letters*, vol. 90, no. 18, p. 185 002, 2003.

[15] B. Albertazzi, J. Béard, A. Ciardi, *et al.*, "Production of large volume, strongly magnetized laser-produced plasmas by use of pulsed external magnetic fields," *Review of Scientific Instruments*, vol. 84, no. 4, p. 043 505, 2013.

[16] D. Higginson, P. Korneev, C. Ruyer, *et al.*, "Laboratory investigation of particle acceleration and magnetic field compression in collisionless colliding fast plasma flows," *Communications Physics*, vol. 2, no. 1, pp. 1–7, 2019.

[17] L. Lancia, M. Grech, S. Weber, *et al.*, "Anomalous self-generated electrostatic fields in nanosecond laser-plasma interaction," *Physics of Plasmas*, vol. 18, no. 3, p. 030 705, 2011.

[18] W. Yao, A. Higginson, J.-R. Marquès, *et al.*, "Dynamics of nanosecond laser pulse propagation and of associated instabilities in a magnetized underdense plasma," *arXiv preprint arXiv:2211.06036*, 2022.

[19] A. Bott, C. Graziani, P. Tzeferacos, *et al.*, "Proton imaging of stochastic magnetic fields," *Journal of Plasma Physics*, vol. 83, no. 6, p. 905 830 614, 2017.

[20] A. Bott, L. Chen, G. Boutoux, *et al.*, "Inefficient magnetic-field amplification in supersonic laser-plasma turbulence," *Physical review letters*, vol. 127, no. 17, p. 175 002, 2021.

[21] H.-K. Chung, M. Chen, W. Morgan, Y. Ralchenko, and R. Lee, "Flychk: Generalized population kinetics and spectral model for rapid spectroscopic analysis for all elements," *High energy density physics*, vol. 1, no. 1, pp. 3–12, 2005.

[22] P. Bolton, M. Borghesi, C. Brenner, *et al.*, "Instrumentation for diagnostics and control of laser-accelerated proton (ion) beams," *Physica Medica*, vol. 30, no. 3, pp. 255–270, May 2014. DOI: 10.1016/j.ejmp.2013.09.002. [Online]. Available: https://doi.org/10.1016/j.ejmp.2013.09.002.

[23] R. Smets, N. Aunai, G. Belmont, C. Boniface, and J. Fuchs, "On the relationship between quadrupolar magnetic field and collisionless reconnection," *Physics of Plasmas*, vol. 21, no. 6, p. 062 111, 2014.

[24] A. Ciardi, S. V. Lebedev, A. Frank, *et al.*, "The evolution of magnetic tower jets in the laboratory," *Physics of Plasmas*, vol. 14, no. 5, p. 056 501, 2007.

[25] G. Gregori, B. Reville, and F. Miniati, "The generation and amplification of intergalactic magnetic fields in analogue laboratory experiments with high power lasers," *Physics Reports*, vol. 601, pp. 1–34, 2015.

[26] A. Colaïtis, D. Turnbull, I. Igumenschev, *et al.*, "3d simulations capture the persistent low-mode asymmetries evident in laser-direct-drive implosions on omega," *Physical Review Letters*, vol. 129, no. 9, p. 095 001, 2022.